Supporting Information

Label-Free SARS-CoV-2 Detection on Flexible Substrates

Debadrita Paria[1,#], Kam Sang Kwok[2,#], Piyush Raj[1], Peng Zheng[1], David H. Gracias [2-7*], Ishan Barman[1,7,8*]

[1]Department of Mechanical Engineering, Johns Hopkins University, Baltimore, MD, USA.

[2]Department of Chemical & Biomolecular Engineering, Johns Hopkins University, Baltimore, MD, USA.

[3]Department of Materials Science and Engineering, Johns Hopkins University, Baltimore, MD, USA.

[4]Department of Chemistry, Johns Hopkins University, Baltimore, MD, USA.

[5] Laboratory for Computational Sensing and Robotics (LCSR). Johns Hopkins University, Baltimore, MD, USA.

[6] Sidney Kimmel Comprehensive Cancer Center (SKCCC), Johns Hopkins University School of Medicine, Baltimore, MD, USA

[7]Department of Oncology, Johns Hopkins University School of Medicine, Baltimore, MD, USA.

[8]Department of Radiology & Radiological Science, Johns Hopkins University School of Medicine, Baltimore, MD, USA

[#]These authors contributed equally to this work.

Keywords: COVID sensors, Surface Enhanced Raman Spectroscopy, Machine Learning, Nano-imprint Lithography, Flexible sensors

***Correspondence:**

David H. Gracias

Johns Hopkins University

Whiting School of Engineering

Department of Chemical & Biomolecular Engineering

Maryland Hall 125

Baltimore, MD 21218, USA

E-mail: dgracias@jhu.edu

Ishan Barman

Johns Hopkins University

Whiting School of Engineering

Department of Mechanical Engineering

Latrobe Hall 103

Baltimore, MD 21218, USA

E-mail: ibarman@jhu.edu

Details of the Finite Element Electromagnetic Simulation Model

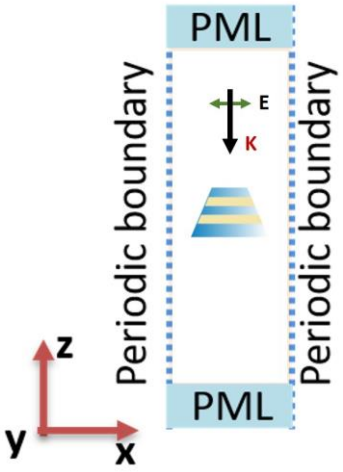

Figure S1: Scheme of simulation. The direction of polarization and the propagation of the incident field is shown by the green and black arrow, respectively.

Absorption characteristics of the FEMIA

From the absorption coefficient an approximate location of the plasmon resonance for the FEMIA with different number of layers can be identified.

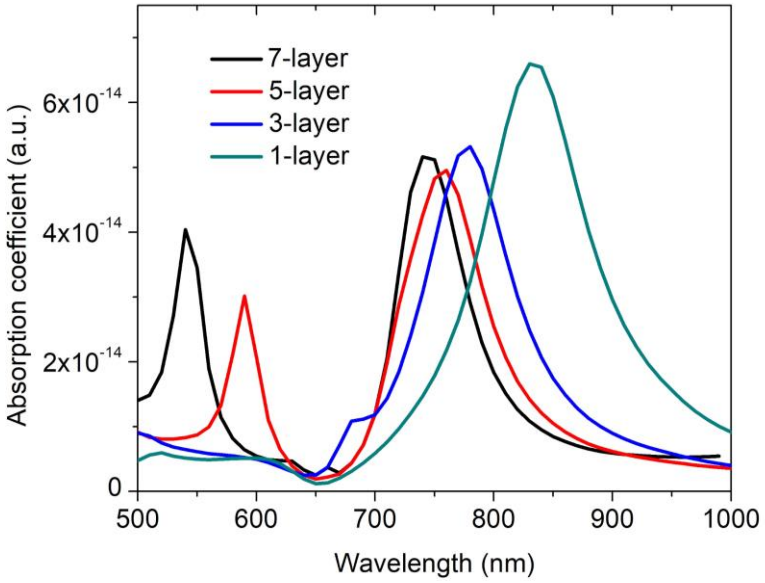

Figure S2: Absorption of a 2-dimensional array of FEMIA nanostructures with a single layer of silver (1 layer), 1 layer of silica sandwiched between 2 layers of silver (3 layer), 2 layer of silica sandwiched between 3 layers of silver with layers alternating (5 layer), 3 layer of silica sandwiched between 4 layers of silver with layers alternating (7 layer).

FEMIA fabrication on rigid (Si) substrate

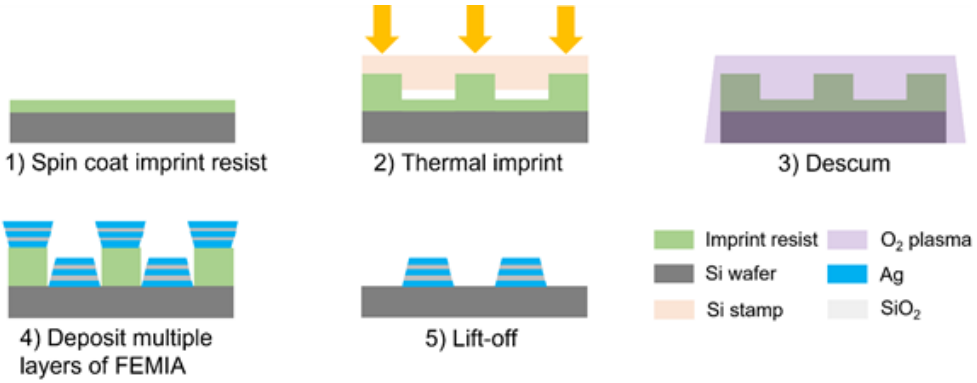

Figure S3: Schematic of the detailed steps for fabrication of FEMIA nanostructures on Si wafer.

FEMIA transfer on flexible substrate

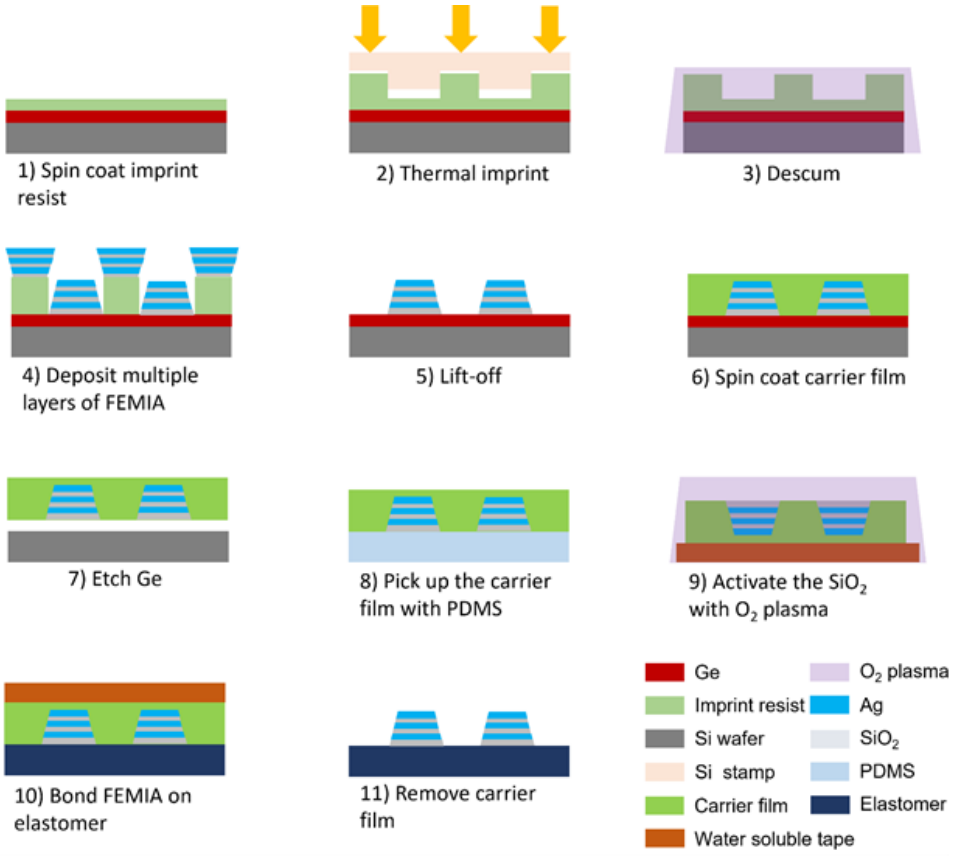

Figure S4: Schematic of the detailed steps for transfer of FEMIA nanostructures on flexible substrates

Dependence of plasmon resonance on array periodicity

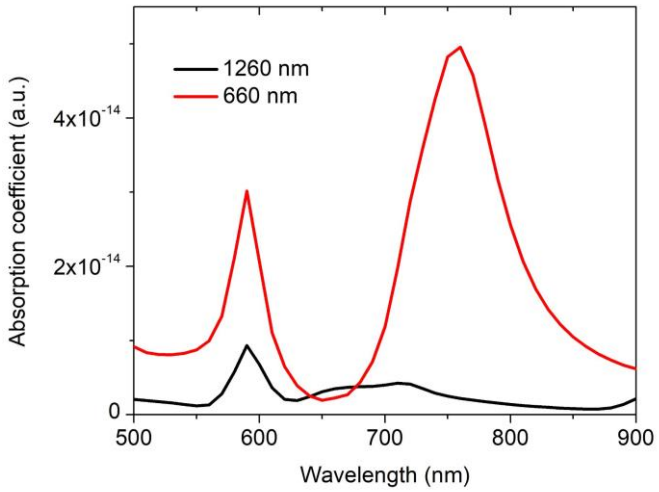

Figure S5: Absorption of an infinite 2-dimensional array of 5-layer FEMIA for different array periodicities, i.e. centre to centre distance of 1260 nm and 660 nm.

Table S1: Peak assignment of the prominent peaks in the Raman spectra of HA and S protein

Raman shift (cm^{-1})	**Assignment**
1048, 1138, 1328, 1621	Tryptophan
1104	Phenylalanine
1155	C-N stretching
1189, 1258	Amide III
1441, 1589	Glycine
1453	C-H stretching of glycoprotein
1567	valine

PCA on SERS spectra of HA and S protein

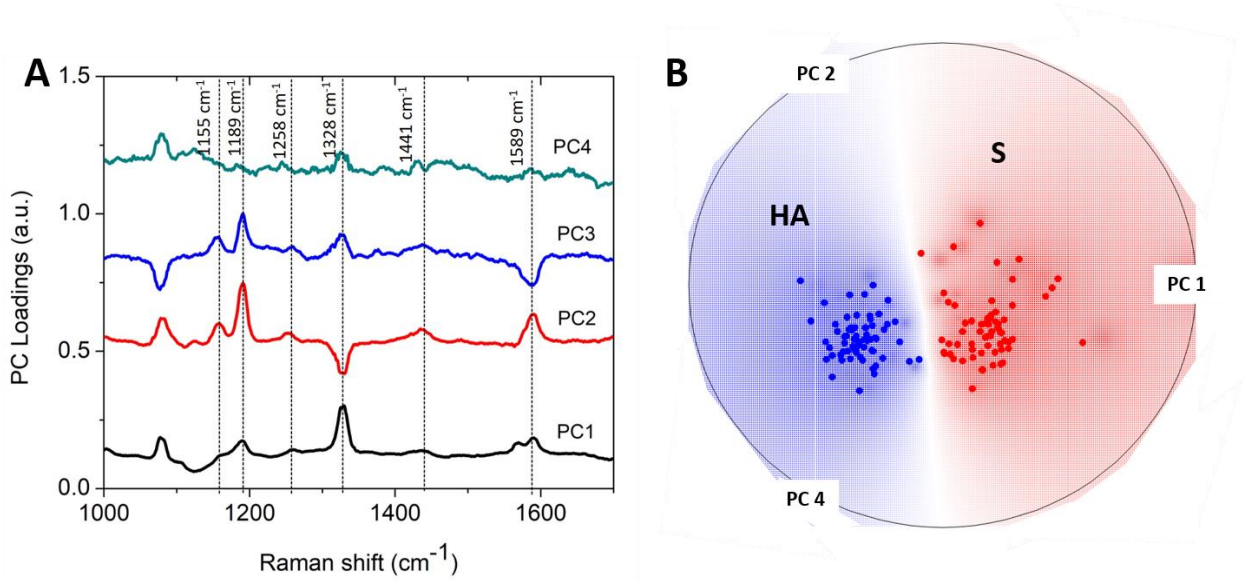

Figure S6: (A) The first four principal components obtained from the entire date set of HA and S protein. The prominent features are represented by the dotted lines. (B) Radial visualization plot of the most relevant PC scores demonstrating the clustering of the two types of proteins.

Dried drop of viral lysate on FEMIA

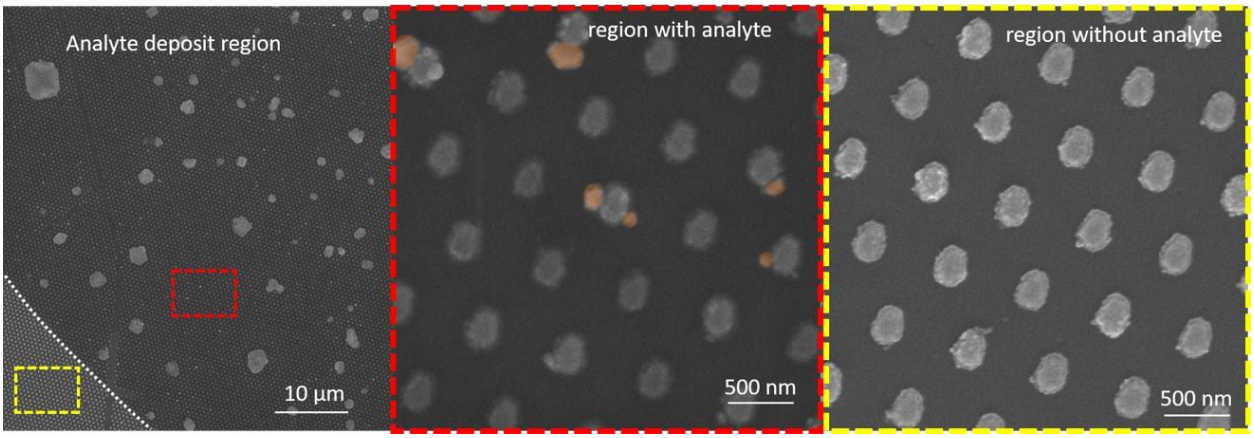

Figure S7: SEM image showing a dried drop of cell lysate infected with SARS-CoV-2 (left panel) on the FEMIA. Zoomed in image of the region with the analyte (middle panel) and without the analyte (right panel). The virus particles are false colored orange for better visualization.

Table S2: Peak assignment of the prominent peaks in the Raman spectra of the cell lysates containing the virus

Raman shift (cm^{-1})	**Assignment**
1004	Phenylalanine
1076	lipids
1123	C-N (protein)
1138, 1622	tryptophan
1156	C-N (protein)
1246, 1280	Amide III
1347	guanine
1367	lipid
1465	adenine

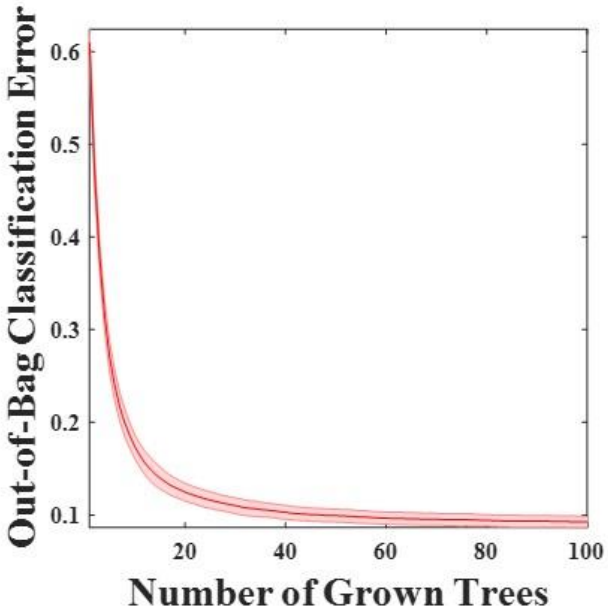

Figure S8: Evaluation of classification error vs number of decision trees, shows that the error falls below 10 % with the inclusion of 100 trees.

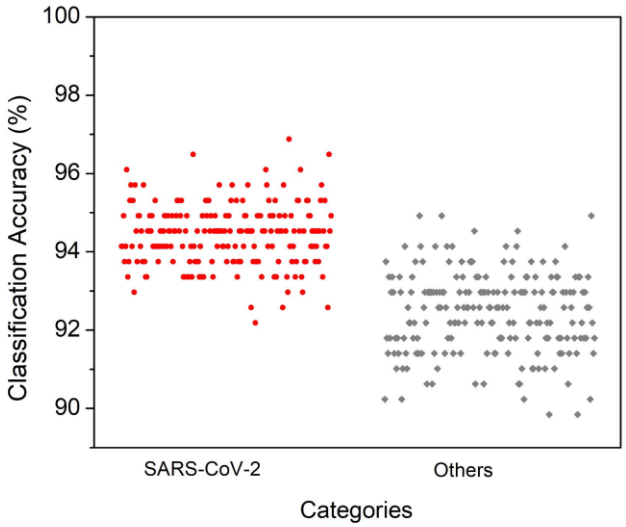

Figure S9: Classification accuracy for binary random forest classification with SARS-CoV-2 sample in one class and the other viruses (H1N1 A, Zika and Marburg) in the other class.